Advanced Healthcare Materials

The effect of gradations in mineral content, matrix alignment, and applied strain on human mesenchymal stem cell morphology within collagen biomaterials

--Manuscript Draft--

Manuscript Number:	adhm.201600181R1
Full Title:	The effect of gradations in mineral content, matrix alignment, and applied strain on human mesenchymal stem cell morphology within collagen biomaterials
Article Type:	Full Paper
Section/Category:	
Keywords:	mesenchymal stem cells; collagen scaffold; cell-matrix interactions; strain; alignment
Corresponding Author:	Brendan Harley, Sc.D. University of Illinois at Urbana-Champaign Urbana, IL UNITED STATES
Additional Information:	
Question	**Response**
Please submit a plain text version of your cover letter here. **If you are submitting a revision of your manuscript, please do not overwrite your original cover letter. There is an opportunity for you to provide your responses to the reviewers later; please do not add them here**.	12 February 2016 Dr. Jos Lenders Advanced Healthcare Materials Email: advhealthmat@wiley-vch.de Dr. Lenders, Attached is a revised version of manuscript adhm.201600181 entitled "The effect of gradations in mineral content, matrix alignment, and applied strain on human mesenchymal stem cell morphology within collagen biomaterials." We appreciate the thoughtful comments of the expert reviewers and have carefully considered their points in preparing an appropriately revised manuscript. We have addressed the comments from all three reviewers in the “Response to Reviewer Comments,” which is attached to this cover letter. The end result is a strengthened and improved paper that we feel is suitable for publication in Advanced Healthcare Materials. I appreciate your consideration of this manuscript and look forward to your response to this revised submission. I encourage you to contact me via the information above if I can provide any additional information to assist in the evaluation of this revised manuscript. Sincerely, Brendan A. Harley Department of Chemical and Biomolecular Engineering Institute for Genomic Biology | Regenerative Biology and Tissue Engineering Department of Materials Science and Engineering Department of Bioengineering Micro and NanoTechnology Laboratory University of Illinois at Urbana-Champaign
Corresponding Author Secondary Information:	
Corresponding Author's Institution:	University of Illinois at Urbana-Champaign
Corresponding Author's Secondary Institution:	
First Author:	Laura C Mozdzen, Masters of Science

First Author Secondary Information:	
Order of Authors:	Laura C Mozdzen, Masters of Science
	Stephen D Thorpe, Ph.D.
	Hazel R.C. Screen, Ph.D.
	Brendan Harley, Sc.D.
Order of Authors Secondary Information:	
Abstract:	The tendon-bone junction (TBJ) is a unique, mechanically dynamic, structurally graded anatomical zone which transmits tensile loads between tendon and bone. Current surgical repair techniques rely on mechanical fixation and can result in high re-failure rates. We have recently described a new class of collagen biomaterial that contains discrete mineralized and structurally aligned regions linked by a continuous interface to mimic the graded osteotendinous insertion. Here we report the combined influence of graded biomaterial environment and increasing levels of applied strain (0 - 20%) on MSC orientation and alignment. In osteotendinous scaffolds, which contain opposing gradients of mineral content and structural alignment characteristic of the native osteotendinous interface, MSC nuclear and actin alignment was initially dictated by the local pore architecture, while applied tensile strain enhanced cell alignment in the direction of strain. Comparatively, in layered scaffolds that did not contain any structural alignment cues, MSCs were randomly oriented in the unstrained condition, then became oriented in a direction perpendicular to applied strain. These findings provide an initial understanding of how scaffold architecture can provide significant, potentially competitive, feedback influencing MSC orientation under applied strain, and forms the basis for future tissue engineering efforts to regenerate the osteotendinous enthesis.

Optional Cover Letter

UNIVERSITY OF ILLINOIS
AT URBANA - CHAMPAIGN

Dr. Brendan A. Harley, Sc.D.
Associate Professor

Department of Chemical and Biomolecular Engineering
Carl R. Woese Institute for Genomic Biology

University of Illinois at Urbana-Champaign

110 Roger Adams Laboratory
600 S. Mathews Avenue, Box C-3
Urbana, Illinois 61801 USA

Phone: (217) 244-7112
Fax: (217) 333-5052
E-mail: bharley@illinois.edu

April 12, 2016

Dr. Jos Lenders
Advanced Healthcare Materials
Email: advhealthmat@wiley-vch.de

Dr. Lenders,

Attached is a revised version of manuscript adhm.201600181 entitled "The effect of gradations in mineral content, matrix alignment, and applied strain on human mesenchymal stem cell morphology within collagen biomaterials." We appreciate the thoughtful comments of the expert reviewers and have carefully considered their points in preparing an appropriately revised manuscript. We have addressed the comments from all three reviewers in the "Response to Reviewer Comments," which is attached to this cover letter. The end result is a strengthened and improved paper that we feel is suitable for publication in *Advanced Healthcare Materials*.

I appreciate your consideration of this manuscript and look forward to your response to this revised submission. I encourage you to contact me via the information above if I can provide any additional information to assist in the evaluation of this revised manuscript.

Sincerely,

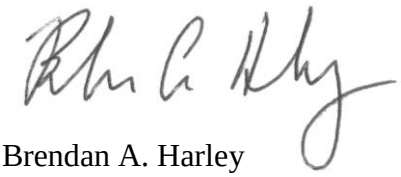

Brendan A. Harley
Assoc. Professor
Department of Chemical and Biomolecular Engineering | Carl R. Woese Institute for Genomic Biology
University of Illinois at Urbana-Champaign
bharley@illinois.edu

WILEY-VCH

DOI: 10.1002/ ((please add manuscript number))
Article type: Full Paper

The effect of gradations in mineral content, matrix alignment, and applied strain on human mesenchymal stem cell morphology within collagen biomaterials

*Laura C. Mozdzen, Stephen Thorpe, Hazel R. Screen, Brendan A. Harley**

L.C. Mozdzen
193 Roger Adams Laboratory
600 S. Mathews St.
Urbana, IL, 61801, USA

S.D. Thorpe
Queen Mary University of London
School of Engineering and Materials Science
Mile End Road, E1 4NS, London, UK

Prof. H.R.C Screen
Queen Mary University of London
School of Engineering and Materials Science
Mile End Road, E1 4NS, London, UK

Prof. B.A.C. Harley
110 Roger Adams Laboratory
600 S. Mathews St
Urbana, IL, 61801, USA
Email: bharley@illinois.edu

Keywords: mesenchymal stem cells, collagen scaffold, cell-matrix interactions strain, alignment

The tendon-bone junction (TBJ) is a unique, mechanically dynamic, structurally graded anatomical zone which transmits tensile loads between tendon and bone. Current surgical repair techniques rely on mechanical fixation and can result in high re-failure rates. We have recently described a new class of collagen biomaterial that contains discrete mineralized and structurally aligned regions linked by a continuous interface to mimic the graded osteotendinous insertion. Here we report the combined influence of graded biomaterial environment and increasing levels of applied strain (0 – 20%) on MSC orientation and alignment. In *osteotendinous* scaffolds, which contain opposing gradients of mineral content and structural alignment characteristic of the native osteotendinous interface, MSC nuclear

and actin alignment was initially dictated by the local pore architecture, while applied tensile strain enhanced cell alignment in the direction of strain. Comparatively, in *layered* scaffolds that did not contain any structural alignment cues, MSCs were randomly oriented in the unstrained condition, then became oriented in a direction perpendicular to applied strain. These findings provide an initial understanding of how scaffold architecture can provide significant, potentially competitive, feedback influencing MSC orientation under applied strain, and forms the basis for future tissue engineering efforts to regenerate the osteotendinous enthesis.

1. Introduction

The tendon-to-bone junction (TBJ) is a unique anatomical zone connecting aligned, elastic tendon to stiff, mineralized bone. TBJ injuries such as in the case of rotator cuff tears are common, with more than 4.5 million physician visits and 250,000 surgeries annually in the US.[1] In a rotator cuff tear, the tendon typically tears away from the bone at the insertion. Surgical fixation is usually via direct anastomosis of the avulsed tendon to bone, resulting in the loss of the characteristic gradients in extracellular matrix proteins, growth factors and mineral content across the insertion. This loss of structural specialization is a primary factor responsible for high (>50%) re-failure rates,[2] motivating development of tissue engineering solutions to improve regenerative healing of the osteotendinous enthesis.

Current technologies for osteotendinous interface repair are inspired by structural and compositional features of the native tissue. Tendons are highly aligned, anisotropic tissues. Like early efforts developing biomaterials for nerve[3] and cardiac[4] tissue repair, the anisotropy of tendon motivated efforts to develop aligned biomaterials for tendon repair, to increase cell proliferation, enhance the maintenance of a tendon phenotype, and improve extracellular matrix production. Aligned biomaterials, with or without the application of tensile strain, have been shown to provide strong structural cues to direct tenocyte alignment

and collagen synthesis,[5] increase MSC proliferation and alignment,[6] and even increased expression levels of tenogenic markers in MSCs and adipose derived stem cells.[7] Similarly, the increased stiffness and mineral content of bone have motivated development of a wide range of mineralized biomaterials with the goal of enhancing MSC osteogenic differentiation.[8]

Regenerative medicine solutions for the TBJ are increasingly turning to the development of biomaterials with complex structural (*e.g.*, pore architecture, alignment), mechanical (*e.g.*, elastic modulus, applied strain), and biomolecular (*e.g.*, mineral content, growth factors) properties, to replicate the complex gradient structure of the junction and subsequently ensure the appropriate guidance of cell bioactivity. Furthermore, given clinical concerns regarding limited expansion of terminally-differentiated cells as well as secondary wound site creation, many efforts are beginning to develop biomaterials to drive mesenchymal stem cell (MSC) differentiation down osteotendinous lineages in a spatially-selective manner.[9] However, in addition to biomaterial-based cues, the function of the native osteotendinous insertion suggests applied tensile strain may be a particularly important instructional signal. Applied strain has previously been shown to alter cell alignment within biomaterials,[10] and in the TBJ is known to underlie initial development of the enthesis.[11] Indeed, while cyclic strain is more commonly used in the context of long-term culture,[12, 13] static strain alone has been shown to induce cellular responses (morphology, alignment).[10, 14] Notably, *Subramony et al.* demonstrated that while mechanical stimulation can alter MSC integrin expression, fibroblast differentiation, and matrix deposition profiles, synergies between mechanical stimulation and alignment can preferentially induce a pro-tenogenic fate.[6]

Unraveling how transitions in biomaterial properties and the application of tensile strain co-regulate MSC activity require the coordination of biomaterial science and imaging. Our lab

has recently described a lyophilization approach to generate three-dimensional collagen-GAG (CG) scaffolds for tendon-to-bone healing applications. We showed anisotropic scaffolds containing structural alignment cues can enhance alignment, proliferation and transcriptomic stability of equine tenocytes,[15, 16] while also selectively activate mechanotransduction paths and MSC tenogenic differentiation in the absence of growth factors supplementation.[9, 17, 18] We have separately demonstrated a hydroxyapatite mineralized CG scaffold that enhanced MSC differentiation towards an osteogenic lineage, again in the absence of conventional osteogenic supplements.[18, 19] We have recently described a method to generate multi-compartment scaffolds that contain discrete scaffold regions connected by a continuous interface.[9] This approach provides orthogonal means to control both the degree of mineralization across the scaffold but also the degree of structural alignment (aligned, non-aligned). This capacity inspires significant questions regarding how cells within a graded scaffold architecture respond to applied strain. Given the graded native osteotendinous insertion, it is critical to establish an approach to examine the coordinated effect of exogenous physical cues such as applied strain and local biomaterial structural cues (pore size, shape) on cell bioactivity.

In this study, we report the collective effect of scaffold structural alignment and applied strain on the alignment and orientation of MSCs within a series of multi-compartment scaffolds inspired by the native tendon-to-bone insertion. The *layered* scaffold variant contained discrete mineralized and non-mineralized compartments, but with an isotropic (non-aligned) pore structure throughout. Comparatively, the *osteotendinous* scaffold also contained discrete mineralized and non-mineralized compartments; however the non-mineralized (tendon) region contained aligned tracks of ellipsoidal pores while the mineralized (bone) compartment contained isotropic pores. Previous work in our lab has shown that aligned, non-aligned, and mineralized scaffold variants all support cell growth and promote long-term (order: weeks)

changes in MSC differentiation,[18] but that matrix anisotropy can influence initial cell alignment within the matrix in the absence of mechanical loading.[15] Given the likely need for tensile stimulation of biomaterials for osteotendinous repair applications, here we evaluate changes in MSC nuclear aspect ratio, nuclear orientation and actin alignment in response to applied tensile stain (0 – 20%) as a function of local scaffold microstructural properties, principally microstructural alignment. We seek to establish a relationship between structural features of *layered* vs. *osteotendinous* scaffolds and initial MSC response to applied stain as the basis for future studies profiling MSC bioactivity in response to long-term bioreactor cultures.

2. Results

2.1 Layered and osteotendinous scaffolds both show graded mineral content but only osteotendinous scaffolds display an aligned pore microstructure

Mean pore size and shape were quantified from both the transverse and longitudinal planes of the *osteotendinous* and *layered* scaffolds (**Figure 1A**) using a previously developed stereology approach in MATLAB.[20] Pore size (**Table 1**) and aspect ratio (**Figure 1B**) varied as a function of mineralized vs. non-mineralized compartment as well as between *layered* and *osteotendinous* scaffold variants. Layered scaffold showed pore sizes in the range of 160 – 230 μm while osteotendinous variants showed pore sizes in the range of 120 – 180 μm, both significantly larger than individual MSCs. Further, both variants displayed an interfacial zone that lacked evidence of voids or areas of delamination (**Figure 1C**), consistent with previous efforts developing these scaffolds.[9] Critical for this work, the *layered* scaffold variant showed no evidence of pore anisotropy in either scaffold compartment. Further, only the non-mineral compartment of the *osteotendinous* scaffold displayed a significant ($p < 0.05$) degree of pore anisotropy (alignment) (**Figure 1B**). Together, these findings confirmed the successful fabrication of two distinct multi-compartment scaffold variants, one that showed a transition

in mineral content (*layered*) and the second that showed a transition from a mineralized, isotropic region to non-mineralized, anisotropic (aligned) region (*osteotendinous*).

2.2 Tracking MSC morphology within the scaffold in response to applied strain

Layered and *osteotendinous* scaffolds were seeded with $6x10^4$ human mesenchymal stem cells (hMSC; passage 6 or less) using a previously defined static seeding method.[21] After which, cell-seeded scaffolds were transferred to custom-made loading chambers fitted to a Leica TCS SP2 laser scanning confocal microscope.[22] This device allowed cell-seeded scaffolds to be maintained in culture media at 37 °C and 5% CO_2 while simultaneously applying defined tensile strain to the entire scaffold (0, 11, 20% strain) for a period of 16 hours, at which cells were fixed and stained for Hoechst (nucleus) and phalloidin (actin).[12] Laser scanning confocal microscopy was used to gather longitudinal image planes from within each scaffold at defined positions, allowing us to examine hMSC nuclear morphology (aspect ratio, orientation) and actin orientation/alignment as a function of scaffold type (*layered* vs. *osteotendinous*), position in the scaffold (mineralized vs. non-mineralized zone) and applied tensile stain (0 vs. 11% vs. 20%) (**Figure 2**).

2.3 hMSC nuclear aspect ratio is heightened and is sensitive to applied tensile strains in scaffolds that contain structural alignment

The experimental setup is summarized in **Figure 2**. hMSC nuclear aspect ratio was significantly affected by both the initial scaffold microstructure and applied strain (**Figure 3**). Notably, while hMSC nuclei were slightly ellipsoidal for all conditions, there was no significant difference in hMSC nuclear aspect ratio in the *layered* scaffold variants as a function of either compartment (mineralized vs. non-mineralized) or applied strain (0 vs. 11% vs. 20%) (**Figure 3A**). However, hMSCs within the *osteotendinous* scaffold showed significant changes in hMSC nuclear aspect ratio as a function of both compartment and applied strain. In the absence of strain, hMSCs in

the (non-aligned) mineralized compartment showed nuclear aspect ratios similar to those seen in the *layered* scaffold, while hMSCs in the (aligned) non-mineralized compartment showed significantly ($p < 0.05$) higher nuclear aspect ratios, a result consistent with previous reports from our group that anisotropic scaffolds induce cell alignment in the absence of strain.[23] However, as strain increased (11, 20%) a more complex behavior emerged. At 11% and 20% strain, both mineralized and non-mineralized compartments of the *osteotendinous* scaffold display higher nuclear aspect ratios than the *layered* scaffolds ($p < 0.01$). Interestingly, at 20% strain, hMSCs in the mineralized compartment of the *osteotendinous* scaffold displayed the highest nuclear aspect ratio (53.7% greater than cells in the same compartment at 0% strain). While not increasing with applied strain, hMSCs in the aligned, non-mineralized compartment still displayed significantly ($p < 0.01$) greater nuclear aspect ratio than hMSCs in the *layered* scaffolds for all stain levels (**Figure 3A)**.

2.4 hMSC nuclear alignment is co-regulated by scaffold microstructural alignment and applied tensile strain

Having established changes in the aspect ratio of the nucleus, we next examined whether the alignment of the nuclei was sensitive to the direction of the applied strain or the scaffold microstructure. Here, data are represented as a half Wind-Rose plot with nuclear alignment histograms generated for angles between -90^o and +90^o (**Figure 3B**). In this representation, 0^o corresponds to the direction of applied strain and the direction of the aligned scaffold microstructure in the non-mineralized compartment of the *osteotendinous* scaffold. Interestingly, hMSCs in the *layered* scaffolds predominantly displayed a significant degree of nuclear orientation in the direction perpendicular to that of applied strain ($p < 0.05$) while the only group which displayed any significant nuclear orientation in the direction of applied strain was in non-mineralized compartment at a physiologically relevant (11%) level of strain ($p < 0.05$). Comparatively, hMSC nuclei in the non-mineralized (aligned) *osteotendinous* scaffold

not only had a higher aspect ratio but also displayed a significant ($p < 0.05$) degree of nuclear alignment coincident with the scaffold architecture even in the absence of strain; comparatively nuclei in the mineralized compartment of the *osteotendinous* scaffold showed no organized alignment. As strain increased, increased nuclear alignment in the direction of strain was observed in both compartments of the *osteotendinous* scaffolds (**Figure 3B**). Together with results regarding nuclear aspect ratio, these data suggest that graded microstructural organization within the *osteotendinous* scaffold provides structural cues that preferentially alter hMSC nuclear shape and alignment even in the absence of strain, but that tensile strain and *osteotendinous* scaffold structural organization together contribute to improved hMSC alignment under physiologically-relevant strain conditions.

2.5 hMSC cytoskeletal response to tensile strain in multi-compartment scaffolds

Given results regarding changes in nuclear shape and alignment, we next examined the degree of actin alignment for hMSCs in the *layered* versus *osteotendinous* scaffolds using a previously described MATLAB analytical technique.[24] Given the differences in nuclear alignment between *layered* and *osteotendinous* scaffolds in response to strain (**Figure 3**), and also the fact that these results were largely unaffected by the level of strain, we compared degree of actin alignment in the mineralized versus non-mineralized compartments of the *layered* (no alignment) versus *osteotendinous* (alignment in the non-mineralized compartment) scaffolds by combining data for all strained conditions (**Figure 4**). Consistent with nuclear data, hMSCs in *layered* scaffolds showed no significant alignment in the direction of strain in either compartment. However, hMSCs in the *osteotendinous* scaffolds showed significant ($p < 0.05$) alignment in the direction of strain in both the non-mineralized and mineralized compartments (**Figure 4**). Together this data suggests that while tensile strain can induce change sin cell alignment on a variety of two-dimensional substrates – often in a direction perpendicular to applied strain,[25] in fully three-dimensional porous scaffolds applied tensile strain affects cell

alignment in a more complex manner that is largely dependent on microstructural features of the underlying scaffold.

3. Discussion

A major focus in the field of orthopedic tissue engineering has been development of biomaterial systems that explore the effect of biomolecular cues[26], biophysical cues[27], or mechanical stimulation cues[28, 29] on mesenchymal stem cell fate, though often exploring these cues singly. However, in vivo a constellation of cues is presented and assimilated by cells. Although some research has begun to explore how matrix stiffness can sensitize stem cells to biomolecular cues,[30] our understanding of how cells incorporate a multitude of signals from different sources is still lacking, but is especially relevant when considering the design of functionally graded biomaterials with the goal of inducing regeneration of complex tissues such as those found in orthopedic interfaces (*e.g.*, osteochondral, osteotendinous).

Here we report the manner in which graded microstructural cues within a scaffold under development for osteotendinous repair applications alters the local response of hMSCs to applied tensile strain. We have previously reported the nature of the graded interface between the mineralized and non-mineralized scaffold regions as being on the order of 100's of microns for both the layered[31] and osteotendinous scaffold variants.[9] For this work, however, we kept our analyses away from the interfacial region so as to examine bulk cell response within the mineralized and non-mineralized zones. Overall, we find that *osteotendinous* scaffolds, which contain transitions in matrix alignment and mineral content, induced a much stronger degree of cellular alignment than *layered* scaffolds, which only contain only a transition in mineral content. hMSC alignment was enhanced in the absence of applied strain in the (aligned) non-mineralized region of the *osteotendinous* scaffold, with increased nuclear aspect ratio, and significant nuclear and actin orientation in the direction of alignment (**Figure 3**). Contrastingly,

we found hMSCs in the *layered* scaffolds that did not contain any structural alignment cues showed a random distribution of nuclear and actin alignment.

Under tensile strain, hMSC nuclear alignment increased but only in the *osteotendinous* scaffolds where anisotropy was initially present. Interestingly, hMSCs in the mineral compartment of the *osteotendinous* scaffold also elicited an increased nuclear aspect ratio, but only after application of strain and even though that scaffold did not present significant degree of pore alignment (**Table 2**). Both actin alignment and nuclear orientation were significantly increased in the direction of applied strain in the *osteotendinous* scaffolds (**Figure 3, 4**). In contrast, hMSCs in the *layered* scaffolds remained randomly oriented under no strain and primarily aligned in a direction perpendicular to that of applied stain, consistent with earlier reports of cell behavior on two-dimensional surfaces where cells attempt to minimize the perceived strain.[25, 32]

Together, these results suggest that pore architecture dictates initial cellular response more than applied strain; an intriguing finding that may inform design of biomaterial-bioreactor systems. These findings also suggests potential differences in cell response to tensile strain in fibrous scaffolds versus in hydrogel constructs, where *Hsieh et al* reported a general increase in alignment in tenocytes in response to static strain.[10] Observed differences in hMSC alignment and response to applied stain found here may be particularly important for osteotendinous regeneration applications. Previous literature has suggested that aligned tissue environments are a key design rule in monolithic (single compartment) biomaterials to enable culture and transcriptomic stability of primary tenocytes,[15, 16, 33] and similarly for inducing early pro-tenogenic differentiation events in MSCs.[18] However, recent literature also suggests anisotropic (aligned) biomaterials may be of added benefit for bone regeneration and tissue ingrowth,[34] making it important to further expand on our finding that hMSCs in the

mineralized compartment of the osteotendinous scaffold also exhibited increased alignment with applied strain. Additional characterization of the stress-relaxation characteristics of the mineralized compartment of the osteotendinous scaffold may provide valuable insight into altered cellular alignment profiles observed in these biomaterials in response to tensile strain.

Given the essential nature of mechanotransduction pathway activation in MSC lineage specification events for range of musculoskeletal, and osteotendinous lineages in particular,[29, 32, 35] it is essential to improve methods to fully describe relationships between mechanical stimulation, biophysical properties of a three-dimensional biomaterial, and resultant MSC bioactivity. In our study, we examined changes in MSC response to a graded scaffold environment in response to static strain. However, recent work from a range of investigators, including our own lab, have demonstrated the particular advantage of cyclic tensile strain for tendon and ligament tissue engineering.[9, 36] New challenges therefore motivate ongoing and future efforts building on the work described here. First, as we have already shown anisotropic scaffolds selectively activate ROCK1 mechanotransduction pathways,[18] ongoing efforts are characterizing local changes in MSC response as a function of position within the scaffold at the signal transduction, gene expression, and protein levels in response to strain. Anisotropic pores are already aligned, and thus cells adhered within the scaffold network may experience a greater degree of strain than isotropic variants. MSCs adhered to scaffold struts not aligned in the direction of strain, and thus not truly experiencing a direct increase in strain, may not experience any stimuli which would elicit a cellular response. Second, dynamic analysis of changes in MSC morphology and subsequent lineage specification would offer an exciting capacity to establish changes in MSC fate as a function of local scaffold biophysical properties and cyclic tensile strain. Our evidence here that MSCs are highly responsive to scaffold architecture and applied tensile strain motivate such ongoing efforts in our laboratory. Thirdly, scaffolds containing a graded transition between compartments offer an ability to examine not

only bulk cellular response as we report here, but also the opportunity to monitor local response across the interfacial zone, with ongoing efforts concentrating on modifying the width and shape of the interfacial zone as well as on dynamically monitoring cell response within the interfacial zone explicitly.

4. Conclusion

In this work, we describe a method to examine changes in the morphology and alignment of hMSCs (nuclear aspect ratio, nuclear orientation, actin alignment) within a three-dimensional collagen biomaterial as a function of both applied strain and local changes in scaffold mineral content and structural alignment. Overall, we found that mesenchymal stem cells within these graded collagen scaffolds respond more strongly to structural alignment cues than applied static strain, suggesting that local control over scaffold pore architecture may be particularly important in the design of biomaterials for musculoskeletal tissue engineering applications. Our results also suggest that a scaffold variant that includes both a transition in mineral content and structural alignment may be of particular interest for applications in osteotendinous insertion repair.

5. Experimental Section

Collagen-glycosaminoglycan (CG) suspension preparation: A CG suspension was prepared from type I collagen (1.0% w/v) isolated from bovine Achilles tendon and chondroitin sulfate (0.1% w/v) derived from shark cartilage in 0.05 M acetic acid (Sigma-Aldrich, St. Louis, MO). The suspension was homogenized at 4 °C to prevent collagen gelatinization during mixing and was degassed before use.[37]

Mineralized CG suspension preparation: A mineralized collagen suspension was prepared from type I collagen (1.93% w/v) isolated from bovine Achilles tendon and chondroitin

sulfate (0.84% w/v) derived from shark cartilage in 0.1456M phosphoric acid / 0.037M calcium hydroxide buffer solution (Sigma-Aldrich, St. Louis, MO). The suspension was homogenized at 4 °C to prevent collagen gelatinization during mixing. Calcium salts ($Ca(OH)_2$ and $Ca(NO_3)\cdot 4H_2O$) were added during homogenization and the suspension was degassed before use. This suspension has previously been shown to produce 40 wt% mineral scaffolds by a titrant-free concurrent mapping method.[38]

Layered scaffold creation: Custom aluminum molds (16 mm x 76 mm) with a removable, flat divider were filled with CG suspension (4.4 mL) in one compartment and mineralized CG suspension (4.4 mL) in the other. The suspension-loaded mold was placed on a freeze-dryer shelf (VirTis, Gardiner, NY) at 20 °C and the divider was removed. The shelf temperature was then ramped down to -40 °C at a rate of 1 °C min^{-1} and held at -40 °C for 1 hour to ensure complete freezing. Following freezing, the shelf temperature was ramped up to 0 °C at a rate of 1 °C min^{-1} while pulling a 200 mTorr vacuum to remove ice crystals via sublimation.[20, 39]

Osteotendinous scaffold creation: Osteotendinous multi-compartment scaffolds were fabricated via lyophilization from a directional solidification method, which has previously been shown to create anisotropic pores.[40] Briefly, the CG suspension was pipetted into a custom polytetrafluoroethylene (PTFE) mold with a copper bottom (wells: 6 mm diameter, 15 mm deep; copper base plate: 1/16” thick), using the thermal mismatch to establish unidirectional heat transfer through the copper bottom, resulting in directionally-aligned ice crystals, and after sublimation directionally-aligned pores. The CG suspension was first pipetted into the PTFE-copper mold, followed by the mineralized CG suspension at a 2:1 volumetric ratio. Both suspensions were allowed to diffuse for approximately 20 minutes and were then placed onto a pre-cooled freeze-dryer shelf (-40 °C). The suspension was then held at -40 °C for 1 hour to ensure complete solidification, and then sublimated at 200 mTorr.[40]

Carbodiimide crosslinking of multi-compartment scaffolds: Prior to use, all scaffolds were hydrated in ethanol followed by phosphate-buffered saline (PBS). They were subsequently crosslinked using carbodiimide chemistry for 1 hour in a solution of 1-ethyl-3-[3-dimethylaminopropyl]carbodiimide hydrochloride (EDC) and N-hydroxysulfosuccinimide (NHS) at a molar ratio of 5:2:1 EDC:NHS:COOH where COOH represents the amount of collagen in the scaffold.[41] After crosslinking, scaffolds were rinsed and stored in PBS until further use.

Quantitative microstructural analysis of multi-compartment scaffolds: Multi-compartment scaffolds (layered and osteotendinous) were cut into pieces no larger than 6 x 10 mm and embedded in glycolmethacrylate. Longitudinal and transverse scaffold sections (5 μm thick) were serially cut via microtome and stained with aniline blue to allow visualization of the collagen-GAG pore structure as previously described.[42] Serial images were then acquired at 10x magnification on an optical microscope (Leica Microsystems, Germany) and mosaically stitched together using Panoramic Tools graphical user interface (PTgui) software to produce a single high resolution image of each scaffold section. Sections from these images were taken depending on image size to ensure at least 10% of the sample was represented. Grayscale image sections were converted to binary images using Ostu's method, which minimizes intra-class variance and is a built-in function in MATLAB. These binary images were further analyzed using a linear intercept script in MATLAB. The script calculated a best-fit ellipse representation of the average pore in each histology section and gave fitting parameters to determine pore size and aspect ratio, the ratio of the major and minor axes of the best-fit ellipse.[20]

SEM analysis of multi-compartment scaffold microstructure: In order to visualize pore elongation within the scaffold variants, longitudinal sections were cut through the scaffolds with a razor blade to expose the interior structure. Scanning electron microscopy (SEM) images of the exposed scaffold face was acquired with a JEOL JSM-6060LV (JEOL, USA) to visualize pore shape within the mineralized, non-mineralized, and interfacial zones of each scaffold variant using a combination of secondary and backscatter electron detection.[16]

HMSC culture: hMSCs used in this experiment were provided by the Knight Group (Queen Mary University of London). They were expanded in complete MSC growth medium at 37 °C and 5% CO_2, and were used prior to passage 6 for all experiments. Multi-compartment scaffolds (layered: 4 mm width, 4 mm thickness, 16 mm length; osteotendinous: 6 mm diameter, 15 mm length) were seeded using a previously established seeding method.[21] Briefly, scaffolds were partially dried with Kimwipes and seeded with $6x10^4$ MSCs in 60 µL of complete MSC media on the top and bottom of each construct (3 aliquots of 20 µL along the length of the scaffold) in six-well plates with 1% agarose gel to prevent cell attachment. Scaffolds were transferred to complete MSC media after a 30 minute attachment period.[40, 43]

Tensile stain: hMSC seeded scaffolds were clamped into a custom tensile stimulation rig, previous described by *Screen* and colleagues.[44] Clamps were positioned to hold the scaffold securely while maintaining a 10 mm gauge-length between clamps at rest.[12] Samples were loaded while the clamps were maintained at 10 mm, being careful not to impart strain to the sample while loading. The chamber was filled with complete MSC medium, with spacers (0 mm, 0.4 mm, 0.7 mm) subsequently inserted to generate the desired degree of static strain (0%, 11%, 20%). Strained scaffolds were maintained at 37 °C and 5% CO_2 for 16 hours prior to analysis.[12]

Nuclear and actin staining: After tensile stimulation, cell-seeded scaffolds were briefly rinsed in PBS then transferred to formalin (Polysciences) overnight at 4 °C. Scaffolds were subsequently rinsed three times in PBS for 1 minute, and then incubated in 0.1% triton X100 for 15 minutes. Scaffolds were rinsed three times in PBS for 1 minute. To resolve actin morphology, scaffolds were incubated in AlexaFluor® 555-phallodin (Invitrogen) dye methanolic stock solution (25 µL in 1 mL PBS) for 30 minutes. Scaffolds were rinsed three times in PBS for 1 minute, and then transferred to a Hoechst (Invitrogen) stock (1 µL in 800 µL PBS) for 5 minutes to label nuclei. Scaffolds were rinsed three times in PBS for 1 minute, transferred to fresh PBS, and stored in the dark at 4°C until imaging.

Confocal imaging of cell-seeded scaffolds: Stained, cell-seeded scaffolds were imaged within 48 hours of fixation using a Leica TCS SP2 laser scanning confocal microscope (Leica Microsystems GmbH, Wetzlar, Germany). Images were acquired using a Leica HC PL Fluotar 20x/0.50na objective using HeNe laser (excitation: 543 nm, collection: 560-700 nm) and UV (collection: 370-535 nm, filter ND50) to image actin and nuclei, respectively. The orientation of the scaffold was maintained so as to generate a series of images (same imaging plane throughout) from the mineralized and non-mineralized regions of the scaffold with a known orientation for applied strain and or scaffold microstructural alignment.

Analysis of hMSC nuclear aspect ratio, orientation: Nuclear aspect ratio and alignment were analyzed from each image using Ovuscule in ImageJ, a macro previously shown to measure the orientation and aspect ratio of elliptical shapes.[45] Ovuscule fits an ellipse to each nucleus, which was then parameterized by three xy-coordinates to define an ellipse function. Ovuscule returns these three xy-coordinates (x1, x2, x3, y1, y2, y3) along with the energy (J), the major and minor axes, and orientation (phi) of the ellipse. Nuclear aspect ratio was determined as ellipsoidal major/minor axis ratio, with nuclear orientation described directly by the

ellipsoidal orientation (phi). Nuclear orientation was then compared to the known orientation of applied strain and scaffold alignment.

Analysis of hMSC cytoskeletal orientation: Fluorescent images of the actin cytoskeleton were analyzed via a previously described MATLAB code to determine the location of actin fibers within the image, followed by localized analysis of the orientation (dominant angle) of that actin fiber [24] Actin orientation was then compared to the known orientation of applied strain and scaffold alignment.

Statistics: All numerical ratios were logarithmically transformed before analysis by one-way ANOVA followed by Tukey post-hoc tests. V-tests were performed on orientation data using the Circular Statistics Toolbox in MATLAB.[46] Significance was set at $p < 0.05$ and error is reported as standard deviation unless otherwise noted. For actin orientation experiments, n = 3 scaffolds comprising a total of n = 12 – 16 images were analyzed per group. For cell nuclei experiments, n = 3 – 7 independent images were analyzed for each group (60 – 400 cells/group).

Acknowledgements

The authors would like to thank Dr. Knight (QMUL) for providing human mesenchymal stem cells for this work, and would also like to acknowledge Dr. Chavaunne Thorpe and Dr. Dharmesh Patel for their guidance. Research reported in this publication was supported by the National Institute of Arthritis and Musculoskeletal and Skin Diseases of the National Institutes of Health under Award Numbers R21 AR063331. LCM was partially funded via National Science Foundation Grant 0965918 *IGERT: Training the Next Generation of Researchers in Cellular & Molecular Mechanics and BioNanotechnology*, which contributed by providing travel support to work with the Screen Lab at Queen Mary University of

London, UK, where a substantial amount of this work took place. LCM also acknowledges support from the University of Illinois via the *Support for Under-Represented Groups in Engineering* (SURGE) Fellowship and the DuPont Science and Engineering Fellowship programs.

Received: ((will be filled in by the editorial staff))
Revised: ((will be filled in by the editorial staff))
Published online: ((will be filled in by the editorial staff))

[1] K. Yamaguchi, K. Ditsios, W. D. Middleton, C. F. Hildebolt, L. M. Galatz, S. A. Teefey, The Journal of Bone & Joint Surgery 2006, 88, 1699.
[2] G. M. Genin, A. Kent, V. Birman, B. Wopenka, J. D. Pasteris, P. J. Marquez, S. Thomopoulos, Biophysical Journal 2009, 97, 976.
[3] Y.-t. Kim, V. K. Haftel, S. Kumar, R. V. Bellamkonda, Biomaterials 2008, 29, 3117; S. Y. Chew, R. Mi, A. Hoke, K. W. Leong, Advanced functional materials 2007, 17, 1288.
[4] E. A. Gonnerman, D. O. Kelkhoff, L. M. McGregor, B. A. C. Harley, Biomaterials 2012, 33, 8812.
[5] A. Kapoor, E. H. G. Caporali, P. J. A. Kenis, M. C. Stewart, Acta Biomater 2010, 6, 2580; C. Chaubaroux, F. Perrin-Schmitt, B. Senger, L. Vidal, J.-C. Voegel, P. Schaaf, Y. Haikel, F. Boulmedais, P. Lavalle, J. Hemmerlé, Tissue Engineering Part C: Methods 2015, 21, 881.
[6] S. D. Subramony, B. R. Dargis, M. Castillo, E. U. Azeloglu, M. S. Tracey, A. Su, H. H. Lu, Biomaterials 2013, 34, 1942.
[7] M. Younesi, A. Islam, V. Kishore, J. M. Anderson, O. Akkus, Advanced Functional Materials 2014, 24, 5762; X. Cheng, C. Tsao, V. L. Sylvia, D. Cornet, D. P. Nicolella, T. L. Bredbenner, R. J. Christy, Acta Biomater 2014, 10, 1360.
[8] T. J. Levingstone, A. Matsiko, G. R. Dickson, F. J. O'Brien, J. P. Gleeson, Acta Biomaterialia 2014, 10, 1996; P. Giannoni, E. Lazzarini, L. Ceseracciu, A. C. Barone, R. Quarto, S. Scaglione, Journal of Tissue Engineering and Regenerative Medicine 2012, n/a.
[9] S. R. Caliari, W. K. Grier, D. W. Weisgerber, Z. Mahmassani, M. D. Boppart, B. A. C. Harley, Advanced healthcare materials 2015, 4, 831.
[10] H.-Y. Hsieh, G. Camci-Unal, T.-W. Huang, R. Liao, T.-J. Chen, A. Paul, F.-G. Tseng, A. Khademhosseini, Lab on a Chip 2013, 14, 482.
[11] P. Jacques, S. Lambrecht, E. Verheugen, E. Pauwels, G. Kollias, M. Armaka, M. Verhoye, A. V. d. Linden, R. Achten, R. J. Lories, D. Elewaut, Ann Rheum Dis 2014, 73, 437.
[12] K. Legerlotz, G. C. Jones, H. R. C. Screen, G. P. Riley, Scand J Med Sci Sports 2013, 23, 31.
[13] H. R. C. Screen, J. C. Shelton, D. L. Bader, D. A. Lee, Biochemical and Biophysical Research Communications 2005, 336, 424; Y. Qiu, J. Lei, T. J. Koob, J. S. Temenoff, Journal of Tissue Engineering and Regenerative Medicine 2014, n/a; N. Chandrashekar, J. Slauterbeck, J. Hashemi, The Knee 2012, 19, 65; S. Saber, A. Y. Zhang, S. H. Ki, D. P. Lindsey, R. L. Smith, J. Riboh, H. Pham, J. Chang, Tissue Engineering Part A 2010, 16, 2085; E. Maeda, Y. Hagiwara, J. H. C. Wang, T. Ohashi, Biomed Microdevices 2013, 15, 1067.

[14] A. Anssari-Benam, D. L. Bader, H. R. C. Screen, Journal of the Mechanical Behavior of Biomedical Materials 2011, 4, 1603; L.-F. Tseng, P. T. Mather, J. H. Henderson, Acta Biomaterialia 2013, 9, 8790.
[15] S. R. Caliari, D. W. Weisgerber, M. A. Ramirez, D. O. Kelkhoff, B. A. C. Harley, J Mech Behav Biomed Mater 2012, 11, 27.
[16] S. R. Caliari, B. A. C. Harley, Biomaterials 2011, 32, 5330.
[17] S. R. Caliari, B. A. C. Harley, Tissue Eng A 2014, 20, 2463.
[18] S. R. Caliari, B. A. C. Harley, Advanced healthcare materials 2014, 3, 1086.
[19] J. C. Lee, C. T. Pereira, X. Ren, W. Huang, D. W. Weisgerber, D. T. Yamaguchi, B. A. C. Harley, T. A. Miller, J Craniofac Surg 2015, 26, 1992; D. W. Weisgerber, S. R. Caliari, B. A. C. Harley, Biomater Sci 2015, 3, 533; X. Ren, D. Bischoff, D. W. Weisgerber, M. S. Lewis, V. Tu, D. T. Yamaguchi, T. A. Miller, B. A. Harley, J. C. Lee, Biomaterials 2015, 50, 107.
[20] F. J. O'Brien, B. A. Harley, I. V. Yannas, L. Gibson, Biomaterials 2004, 25, 1077.
[21] F. J. O'Brien, B. A. Harley, M. A. Waller, I. V. Yannas, L. J. Gibson, P. J. Prendergast, Technology and Health Care 2007, 15, 3.
[22] H. R. Screen, D. A. Lee, D. L. Bader, J. C. Shelton, Proc Inst Mech Eng H 2004, 218, 109.
[23] S. Caliari, B. Harley, In Preparation 2014.
[24] W. J. Karlon, P.-P. Hsu, S. Li, S. Chien, A. D. McCulloch, J. H. Omens, Annals of Biomedical Engineering 1999, 27, 712.
[25] Z. Wei, V. S. Deshpande, R. M. McMeeking, A. G. Evans, J Biomech Eng 2008, 130, 031009.
[26] A. Matsiko, T. J. Levingstone, J. P. Gleeson, F. J. O'Brien, Advanced Healthcare Materials 2015, 4, 1175; H. K. Min, S. H. Oh, J. M. Lee, G. I. Im, J. H. Lee, Acta Biomaterialia 2014, 10, 1272; J. Halper, in *Progress in Heritable Soft Connective Tissue Diseases*, (Ed: J. Halper), Springer Netherlands, 2014, 59.
[27] T. H. Kim, D. B. An, S. H. Oh, M. K. Kang, H. H. Song, J. H. Lee, Biomaterials 2015, 40, 51; J. R. Gershlak, J. I. Resnikoff, K. E. Sullivan, C. Williams, R. M. Wang, L. D. Black, 3rd, Biochem Bioph Res Co 2013, 439, 161.
[28] D. W. Youngstrom, I. Rajpar, D. L. Kaplan, J. G. Barrett, Journal of Orthopaedic Research 2015, 33, 911; C. Popov, M. Burggraf, L. Kreja, A. Ignatius, M. Schieker, D. Docheva, BMC Mol Biol 2015, 16; Y. Xu, Q. Wang, Y. Li, Y. Gan, P. Li, S. Li, Y. Zhou, Q. Zhou, Biomed Res Int 2015, 2015, 790804; T. Wang, Z. Lin, M. Ni, C. Thien, R. E. Day, B. Gardiner, J. Rubenson, T. B. Kirk, D. W. Smith, A. Wang, D. G. Lloyd, Y. Wang, Q. Zheng, M. H. Zheng, Journal of Orthopaedic Research 2015, n/a.
[29] J. Hao, Y. Zhang, D. Jing, Y. Shen, G. Tang, S. Huang, Z. Zhao, Acta Biomaterialia 2015, 20, 1.
[30] J. H. Wen, L. G. Vincent, A. Fuhrmann, Y. S. Choi, K. C. Hribar, H. Taylor-Weiner, S. Chen, A. J. Engler, Nature Materials 2014, 13, 979; J. L. Allen, M. E. Cooke, T. Alliston, Mol Biol Cell 2012, 23, 3731; O. F. Zouani, J. Kalisky, E. Ibarboure, M.-C. Durrieu, Biomaterials 2013, 34, 2157; J. M. Banks, L. C. Mozdzen, B. A. C. Harley, R. C. Bailey, Biomaterials 2014, 35, 8951.
[31] B. A. Harley, A. K. Lynn, Z. Wissner-Gross, W. Bonfield, I. V. Yannas, L. J. Gibson, J Biomed Mater Res A 2010, 92, 1078; D. W. Weisgerber, D. O. Kelkhoff, S. R. Caliari, B. A. C. Harley, J Mech Behav Biomed Mater 2013, 28, 26.
[32] K. Kurpinski, J. Chu, C. Hashi, S. Li, Proc Natl Acad Sci U S A 2006, 103, 16095.
[33] A. Kapoor, E. H. Caporali, P. J. Kenis, M. C. Stewart, Acta Biomater 2010, 6, 2580; E. Caporali, A. Kapoor, P. A. Kenis, M. C. Stewart, "TGF-β and microtopographical cues promote expression of tenogenic marker genes and tenocyte alignment.", presented at *Proceedings of the 36th Annual Conference of the Veterinary Orthopedic Society*, 2009.

[34] P. Joly, G. N. Duda, M. Schone, P. B. Welzel, U. Freudenberg, C. Werner, A. Petersen, PLoS One 2013, 8, e73545; J. Kopf, A. Petersen, G. N. Duda, P. Knaus, BMC Biol 2012, 10, 37; N. Davidenko, T. Gibb, C. Schuster, S. M. Best, J. J. Campbell, C. J. Watson, R. E. Cameron, Acta Biomater 2012, 8, 667; J. Li, F. You, Y. Li, Y. Zuo, L. Li, J. Jiang, Y. Qu, M. Lu, Y. Man, Q. Zou, J Biomater Sci Polym Ed 2016, 27, 327.
[35] B. Xu, G. Song, Y. Ju, X. Li, Y. Song, S. Watanabe, J Cell Physiol 2012, 227, 2722; D. Marolt, A. Augst, L. E. Freed, C. Vepari, R. Fajardo, N. Patel, M. Gray, M. Farley, D. Kaplan, G. Vunjak-Novakovic, Biomaterials 2006, 27, 6138.
[36] Y. Qiu, J. Lei, T. J. Koob, J. S. Temenoff, J Tissue Eng Regen Med 2014; J. Z. Paxton, P. Hagerty, J. J. Andrick, K. Baar, Tissue Eng Part A 2012, 18, 277; Y. Morita, S. Watanabe, Y. Ju, B. Xu, Acta of bioengineering and biomechanics / Wroclaw University of Technology 2013, 15, 71; H. R. C. Screen, S. R. Byers, A. D. Lynn, V. Nguyen, D. Patel, S. J. Bryant, Adv Funct Mater 2010, 20, 738.
[37] I. V. Yannas, E. Lee, D. P. Orgill, E. M. Skrabut, G. F. Murphy, Proc Nat Acad Sci 1989, 86, 933.
[38] A. K. Lynn, S. M. Best, R. E. Cameron, B. A. Harley, I. V. Yannas, L. J. Gibson, W. Bonfield, Journal of Biomedical Materials Research Part A 2010, 92A, 1057; D. W. Weisgerber, D. O. Kelkhoff, S. R. Caliari, B. A. C. Harley, Journal of the Mechanical Behavior of Biomedical Materials 2013, 28, 26.
[39] B. Harley, J. Leung, E. Silva, L. Gibson, Acta Biomater 2007, 3, 463.
[40] S. R. Caliari, B. A. C. Harley, Biomaterials 2011, 32, 5330.
[41] C. M. Murphy, A. Matsiko, M. G. Haugh, J. P. Gleeson, F. J. O'Brien, J Mech Behav Biomed 2012, 11, 53; D. Spillmann, U. Lindahl, Current Opinion in Structural Biology 1994, 4, 677.
[42] F. J. O'Brien, B. A. Harley, I. V. Yannas, L. Gibson, Biomaterials 2004, 25, 1077.
[43] F. J. O'Brien, B. A. Harley, I. V. Yannas, L. J. Gibson, Biomaterials 2005, 26, 433.
[44] K. Legerlotz, G. C. Jones, H. R. C. Screen, G. P. Riley, Scand J Med Sci Sports 2013, 23, 31; A. Anssari-Benam, H. S. Gupta, H. R. Screen, J Biomech Eng 2012, 134, 061003; H. R. C. Screen, T. Demirci, A. Lynn, A. Blackney, D. Patel, S. J. Bryant, Int J Exp Pathol 2011, 92, A11.
[45] P. Thévenaz, R. Delgado-Gonzalo, M. Unser, IEEE Transactions on Pattern Analysis and Machine Intelligence 2011, 33, 382.
[46] P. Berens, J Stat Softw 2009, 31, 1.

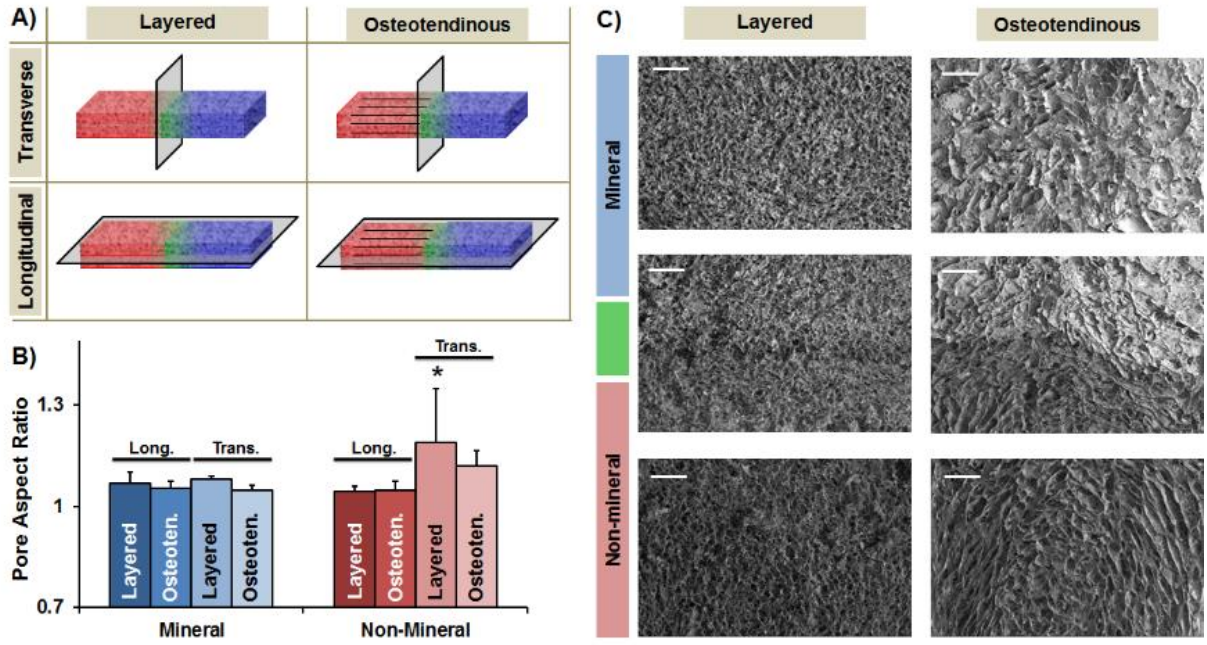

Figure 1. Pore architecture of layered and osteotendinous scaffold variants. A) Schematic of histology slices relative to whole scaffolds (left: osteotendinous; right: layered; top: transverse; bottom: longitudinal) **B)** Transverse and longitudinal pore aspect ratio in layered and osteotendinous scaffolds. *: significantly greater than all other values ($p<0.05$) **C)** Scanning electron microscope images of pore architecture at the in discrete mineral (top) and non-mineral (bottom) compartments, in addition to the interface where both compartments meet (middle). Images are displayed for both layered (left) and osteotendinous (right) scaffolds. Cell orientation was not quantified at the insertion between compartments (green). Scale bar: 500 µm

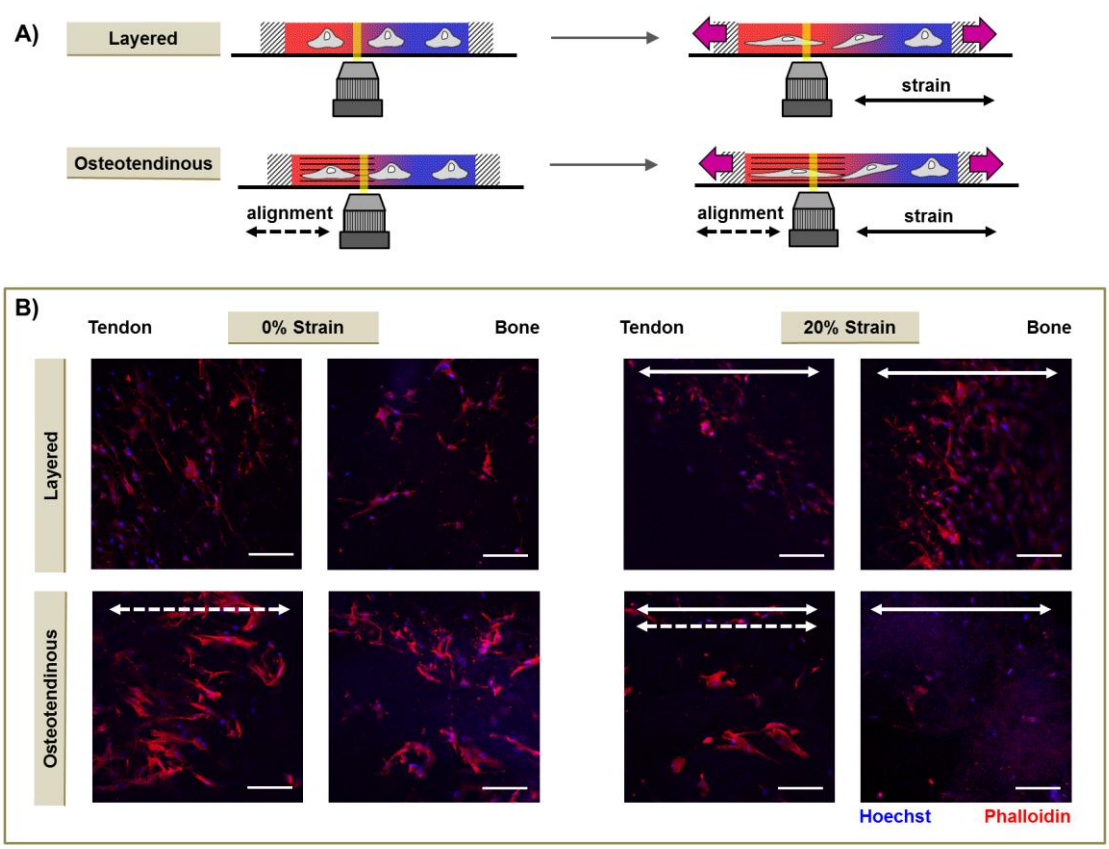

Figure 2. Schematic of experimental design and representative images acquired from non-mineralized (tendon) and mineralized (bone) regions of the layered vs. osteotendinous scaffold variants under applied strain. A) Layered scaffolds (containing a mineralized and non-mineralized regions but no microstructural alignment) and osteotendinous scaffolds (containing mineralized and structurally-aligned non-mineralized regions) were seeded with MSCs then cultured overnight in the presence of discrete levels of applied stain (0%, 11%, 20%). Scaffolds were stained with Hoechst (nuclei) and/or Phalloidin (actin), then viewed on a confocal microscope to quantify cell response (nuclear and cytoskeletal alignment) as a function of local scaffold properties. **B)** Representative images of actin (phalloidin) and nuclear (Hoechst) staining on hMSCs seeded on multi-compartment scaffolds with or without alignment and with increasing strain. Scale bar: 100 µm.

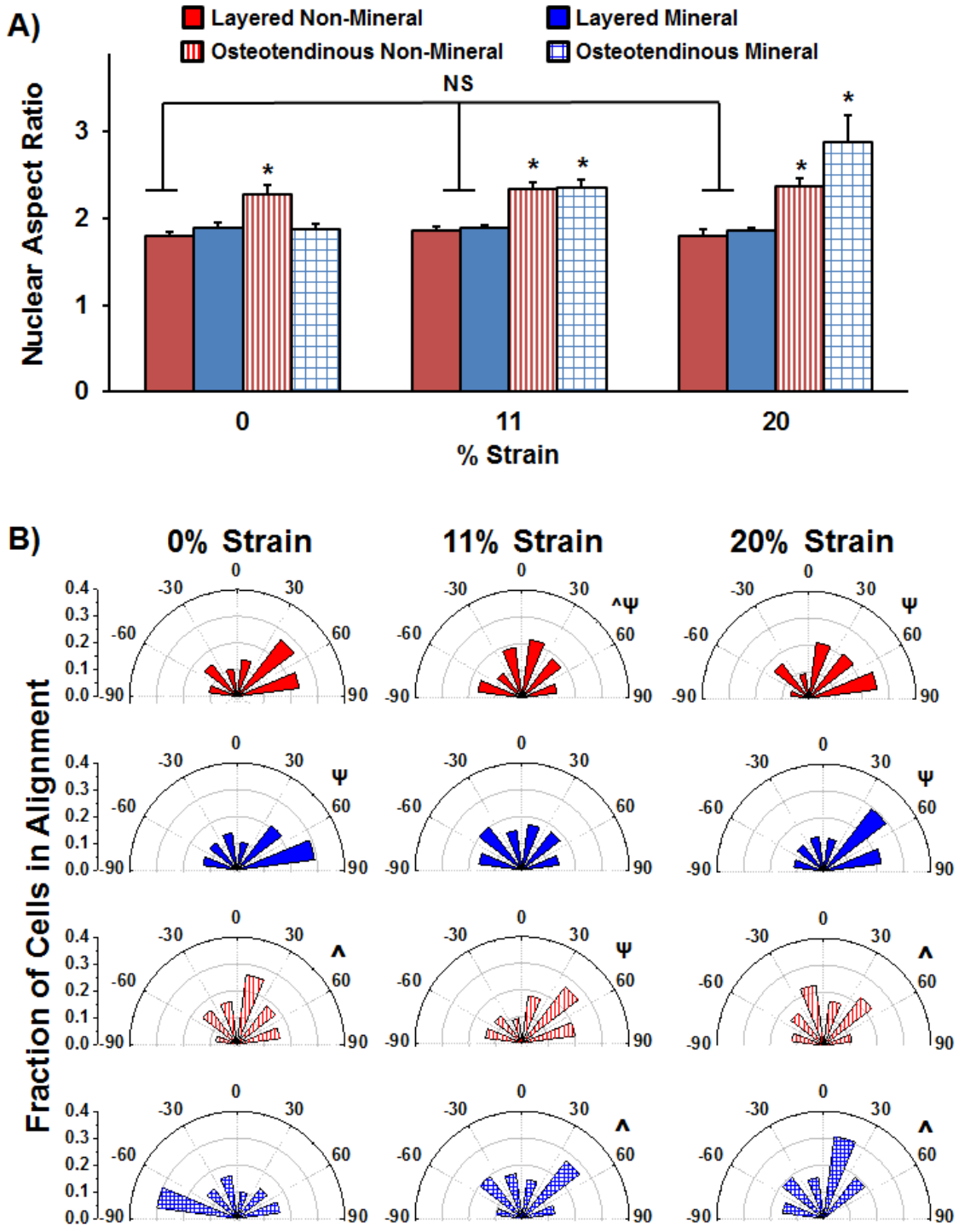

Figure 3. Cellular response to scaffold structural variation and increasing strain. A) Overnight strain impacts nuclear aspect ratio in osteotendinous scaffolds, but has no effect in layered scaffold variants. *: significantly greater than layered counter-part ($p<0.05$) **B)** Nuclear orientation in (top to bottom) layered and osteotendinous scaffolds with increasing strain. In layered scaffolds, significant nuclear alignment perpendicular to the applied strain was found consistently; in osteotendinous scaffolds, significant nuclear alignment in the direction of applied strain was found consistently. ^: significantly aligned with strain (0 degrees; $p<0.05$); Ψ: significantly aligned perpendicular to strain (90 degrees; $p<0.05$)

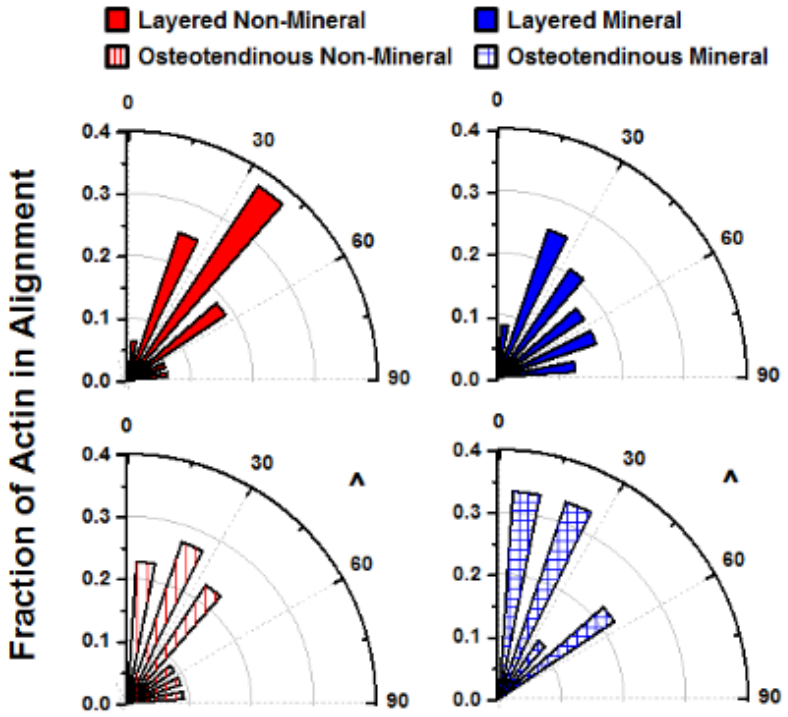

Figure 4. Actin alignment in layered and osteotendinous scaffolds after strain. Actin fibers were significantly oriented in the direction of applied strain only in the osteotendinous scaffold variants. ^: significantly aligned with strain (0 degrees; $p < 0.05$)

Table 1. Mean scaffold pore size for both layered and osteotendinous scaffolds. Pore sizes are reported as mean ± standard deviation for both the transverse and longitudinal planes within each scaffold compartment.

Scaffold Variant	Compartment	Transverse Pore Size [µm]	Longitudinal Pore Size [µm]
Layered	Mineral	166 ± 33.7	256 ± 64.7
	Non-Mineral	175 ± 27.6	227 ± 37.9
Osteotendinous	Mineral	183 ± 10.6	182 ± 39.1
	Non-Mineral	125 ± 18.1	137 ± 10.9

Table 2. Mean scaffold pore aspect ratio within layered and osteotendinous scaffolds. Pore aspect ratios are reported as mean ± standard deviation for both the transverse and longitudinal planes within each scaffold compartment.

Scaffold Variant	Compartment	Transverse Pore Aspect Ratio	Longitudinal Pore Aspect Ratio
Layered	Mineral	1.05 ± 0.02	1.07 ± 0.03
	Non-Mineral	1.05 ± 0.02	1.04 ± 0.01
Osteotendinous	Mineral	1.10 ± 0.03	1.08 ± 0.02
	Non-Mineral	1.12 ± 0.04	1.19 ± 0.16

We report the effect of transitions in pore anisotropy and mineral content across three-dimensional collagen scaffolds on MSC alignment in response to tensile strain. MSCs align consistently in the direction of local pore architecture, though in response to strain cells in isotropic scaffolds orient perpendicular to strain. Scaffold pore architecture provides significant structural feedback influencing MSC orientation under strain.

Keyword: mesenchymal stem cells, collagen scaffold, cell-matrix interactions strain, alignment

Laura C. Mozdzen, Stephen Thorpe, Hazel R. Screen, Brendan A. Harley*

The effect of gradations in mineral content, matrix alignment, and applied strain on human mesenchymal stem cell morphology within collagen biomaterials

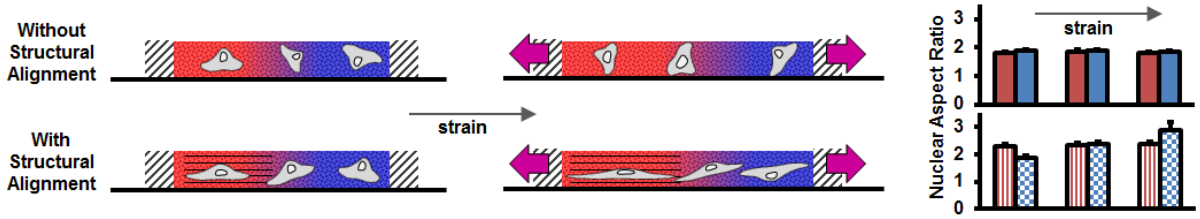

Manuscript, Table of Contents Figure